Progress In Electromagnetics Research B, Vol. 72, 31–47, 2017

Electromagnetic Scattering from Bi-Periodic Fabric Structures

Mohammad Mahdi Salary, Samad Jafar-Zanjani, and Hossein Mosallaei*

Abstract—We develop an efficient semi-analytical technique to calculate the electromagnetic scattering from fabric structures modeled as crossed gratings of circular coated fibers of any material composition, arranged arbitrarily in yarns. The method relies on a matrix formulation based on multipole expansion for modeling conical scattering from uniaxial gratings of fibers, and employs a scattering matrix approach to obtain co- and cross-polarized transmission and reflection coefficients. The lattice sums are evaluated using an efficient adaptive algorithm based on Shank's transformation. The method can be employed for analyzing the scattering characteristics of fabric structures embedded in any arbitrary layered media. The validity of the method is verified through comparison with full-wave finite-difference time-domain simulations. A substantial performance gain is obtained, which makes the proposed method applicable to solve large-scale fabric structures.

1. INTRODUCTION

Interaction of electromagnetic waves with textiles and fabric structures is currently of significant importance for several different applications such as personal thermal management [1, 2], wearable energy harvesting [3, 4], solar-cell carpeting [5, 6], shielding against hazardous radiations [7, 8] and medical dressings [9, 10]. Moreover, such structures can be regarded as constituent layers of 3D photonic crystals and woodpile structures. The modern fabrication technologies offer a great amount of flexibility in modification of composite fabric structures and open up several exciting opportunities for design and optimization of technical fabrics and fiber-based devices.

Along with the rapid progress in fabrication techniques, there is a need to improve numerical simulation techniques to further speed up the design and optimization processes. The necessary step for modeling the fabric structures given as bi-periodic arrays of circular cylinders (fibers) arranged in bundles (yarns), is solving the problem of scattering from cylinders. This problem has been studied for many years and several different methods have been adopted for this purpose [11–25]. Some of these are general methods, such as the finite-difference time-domain (FDTD) method [11], finite-element method (FEM) [12], boundary-element method [13] and rigorous coupled waveguide analysis (RCWA) [14]. However, the unit-cell of such fabric structures might be extended over many optical wavelengths which inevitably leads to numerical models with enormous numbers of unknowns, considering small geometrical features that necessitate ultra-fine meshing.

Therefore, semi-analytical methods that exploit some available geometrical features of the structure can be of great advantage [15–30]. These methods rely on the multipole expansions and often outperform full-wave methods particularly when the number of elements is large and the number of excited modes inside each element could be kept small [31]. Among the various multipole expansion techniques, T-matrix is the most powerful method due to its simplicity and generality. The problem of electromagnetic scattering form an arbitrarily shaped homogeneous scatterer was formulated by Waterman, based on

Received 31 October 2016, Accepted 9 December 2016, Scheduled 22 December 2016

* Corresponding author: Hossein Mosallaei (hosseinm@ece.neu.edu).

The authors are with the Computational EM and Physics Lab, Electrical and Computer Engineering Department, Northeastern University, Boston, MA 02115, USA.

the T-matrix method [27]. Peterson and Strom [28, 29] extended this formulation to the case of an arbitrary number of 2D scatterers by applying the translation formula to the cylindrical wave solution of Helmoltz's wave equation. Later, Chew [30, 31] developed a generalized recursive algorithm to calculate the scattered field by multiple scatterers. This technique is well adapted to solve several problems involving cylindrical structures [32–38], however, it is limited to ideal 2D problems where both the structure and the incidence geometries are invariant in one direction leading to scalar 2D problems involving the E and H polarizations separately. For the out-of-plane propagation problems, one might use 3D T-matrix formulation in conjunction with extended boundary conditions method (EBCM) [39] which entails considerably more effort. However, since the structure is 2D, one can still formulate the problem using vector cylindrical harmonics and obtain a similar matrix formulation at the cost of dependency on the incidence [24–26].

Consider a non-interlaced fabric structure as shown in Fig. 1. In this work, we present a 2D treatment of such 3D geometry. A robust matrix formulation for modeling conical scattering from periodic gratings of coated fibers arranged arbitrarily in the bundles is developed which can be regarded as a major extension of the T-matrix method. The lattice sums involving the translation of harmonics for on-axis and off-axis periodicity are evaluated using an efficient adaptive algorithm based on Shank's transformation. Next, the scattering matrix approach is employed to obtain co- and cross-polarized diffraction efficiencies of the fabric structures consisted of stack of crossed grating layers where each layer is invariant in one direction.

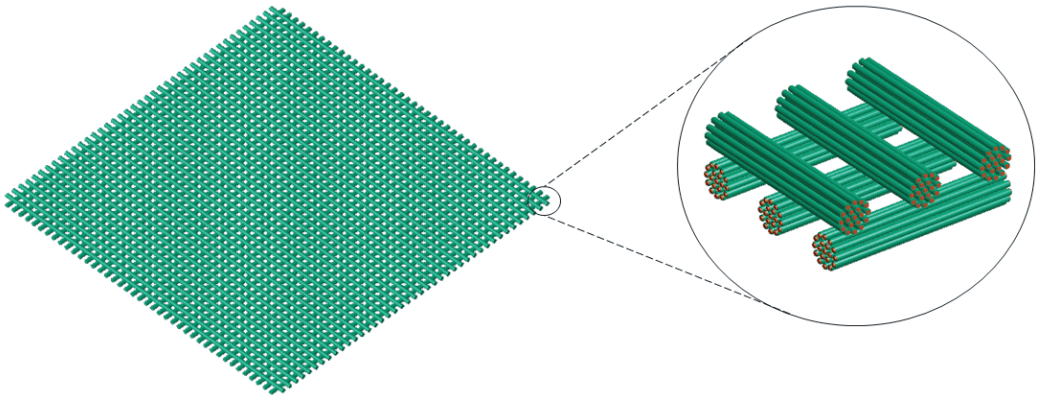

Figure 1. The schematic representation of a non-interlaced fabric structure, comprising of core-shell fibers bundled up into yarns, along with an outset zoom-in plot.

The overall procedure of the method is depicted as a flow-chart in Fig. 2. This treatment is a major extension of [40, 41] which have studied the woodpile structures where the unit-cell of the grating contains only one cylinder. It should be remarked that unlike the super-cell methods, the proposed method requires periodicity only in the directions of the gratings but not in the stacking direction and, thus, is applicable for a finite number of layers. The method is appropriate for efficient modeling large-scale fabric structures embedded in any arbitrary layered media. Furthermore, it can treat arbitrary arrangements of coated fibers made of dielectric and metallic materials within the unit-cell with equal ease.

In Section 2, we establish the procedure for modeling fabric structures and present our formulation. Numerical examples are given in Section 3 to demonstrate the applicability of the method and the results are compared with full-wave simulations to verify validity and efficiency of the method.

2. FORMULATION

2.1. Conical Scattering from Gratings of Fibers: Multipole Expansion

We start the mathematical formulation by considering a periodic grating of an arbitrary arrangement of uniaxial coated fibers, invariant in the z direction, illuminated by an oblique plane wave as shown in

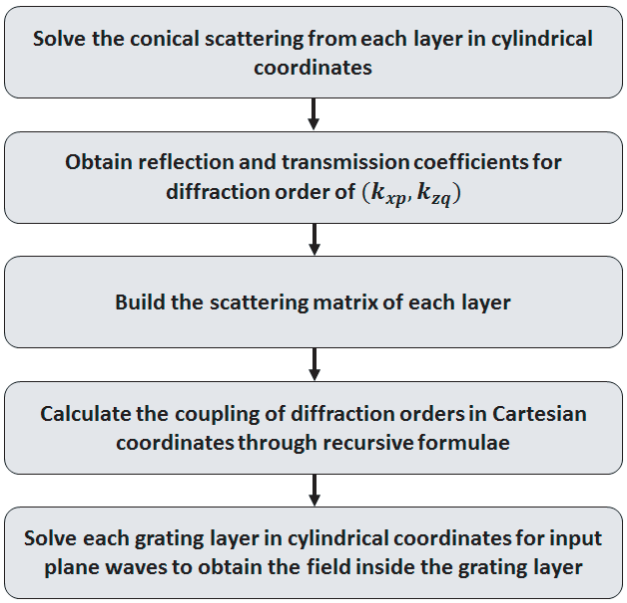

Figure 2. The flow-chart of the overall procedure in the proposed method for calculating the electromagnetic scattering form bi-periodic fabric structures.

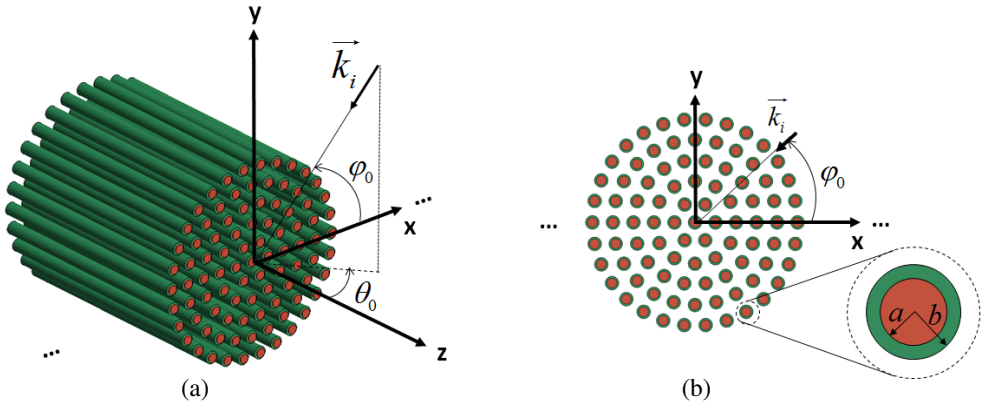

Figure 3. A periodic grating of an arbitrary arrangement of uniaxial coated fibers, (a) 3D Geometry, (b) x-y, 2D cross-sectional geometry.

Fig. 3. The 0-th unit-cell is the reference cell which is repeated periodically in the x-axis direction with a periodicity Λ. The repeated unit-cells are shown with the indices $j = -\infty, \ldots, -1, +1, \ldots, +\infty$. The filling fraction of the core-shells within the unit-cell and their corresponding electromagnetic parameters can be different in this model. The in-plane and out-of-plane incidence angles are denoted by ϕ_0 and θ_0, respectively. We introduce local coordinate systems $(x_{j,l}, y_{j,l})$ located at the centers of the l-th fiber within j-th cell. The corresponding polar coordinates are denoted by $(\rho_{j,l}, \phi_{j,l})$. The time convention is assumed to be $\exp(-i\omega t)$ throughout the paper.

The transverse magnetic (TM^z) polarization corresponds to the case where the electric field is perpendicular to the incidence plane. The z component of the incident electric field can be written as:

$$E^{(i),\mathrm{TM}} = E_0 \sin\theta \exp[i(k_{0x}x - k_{0y}y + k_{0z}z)] \tag{1}$$

Similarly, for the transverse electric (TE^z) polarization where the electric field is parallel to the

incidence plane, the z component of the incident magnetic field can be expressed as:

$$H^{(i),\mathrm{TE}} = H_0 \sin\theta \exp[i(k_{0x}x - k_{0y}y + k_{0z}z)] \tag{2}$$

In the above equations E_0 and H_0 are normalizing amplitudes and:

$$k_0 = 2\pi/\lambda \tag{3}$$
$$k_{0x} = k_0 \sin\theta_0 \cos\phi_0 \tag{4}$$
$$k_{0y} = -k_0 \sin\theta_0 \sin\phi_0 \tag{5}$$
$$k_{0z} = k_0 \cos\theta_0 \tag{6}$$

The incident fields can be expanded in terms of cylindrical harmonics in the local coordinate system of l-th cylinder inside the 0-th unit-cell as:

$$E_l^{(i),\mathrm{TM}} = \sum_{m=-\infty}^{+\infty} a_m^{(i),E,l} J_m(k_{0t}\rho_{0,l}) e^{-im\phi_{0,l}} \tag{7}$$

$$H_l^{(i),\mathrm{TE}} = \sum_{m=-\infty}^{+\infty} a_m^{(i),H,l} J_m(k_{0t}\rho_{0,l}) e^{-im\phi_{0,l}} \tag{8}$$

where:

$$k_{0t} = \sqrt{k_0^2 - k_{0z}^2} = \sqrt{k_{0x}^2 + k_{0y}^2}; \tag{9}$$
$$a^{(i),E,l} = E_0 \sin\theta (-i)^n e^{in\phi_0} \exp[i(k_{0x}x_l - k_{0y}y_l + k_{0z}z_l)] \tag{10}$$
$$a^{(i),H,l} = H_0 \sin\theta (-i)^n e^{in\phi_0} \exp[i(k_{0x}x_l - k_{0y}y_l + k_{0z}z_l)] \tag{11}$$

Then, the z component of the scattered fields from l-th cylinder inside n-th unit-cell can then be expressed in the following form for an arbitrary linear combination of TM and TE incidence:

$$E_{n,l}^{(s)} = \sum_{m=-\infty}^{+\infty} b_m^{(s),EE,l} H_m^{(1)}(k_{0t}\rho_{n,l}) e^{-im\phi_{n,l}} + \sum_{m=-\infty}^{+\infty} b_m^{(s),EH,l} H_m^{(1)}(k_{0t}\rho_{n,l}) e^{-im\phi_{n,l}} \tag{12}$$

$$H_{n,l}^{(s)} = \sum_{m=-\infty}^{+\infty} c_m^{(s),HH,l} H_m^{(1)}(k_{0t}\rho_l) e^{-im\phi_l} + \sum_{m=-\infty}^{+\infty} c_m^{(s),HE,l} H_m^{(1)}(k_{0t}\rho_l) e^{-im\phi_l} \tag{13}$$

All the other components of the field can be obtained through application of Maxwell's equations.

2.2. Enforcing Boundary Conditions: Matrix Formulation

As mentioned earlier, T-matrix method is not applicable in this case. However, we can extend the matrix formulation at the cost of dependency of the transition matrix on the incidence. Here, we are dealing with cross-polarized coupling because of the out-of-plane variation of the incident field. If the fibers are invariant in the z-direction, the grating will conserve k_{0z} and all the field contributions will have the same z-dependence. This allows us to work only with the z-component of the fields. Following the procedure of T-matrix method, we define following basis column vectors

$$\left[\overline{\psi}(k_{0t}\rho_{n,l}, \phi_l)\right]_m = H_m^{(1)}(k_{0t}\rho_{n,l}) e^{-im\phi_{n,l}} \tag{14}$$
$$\left[\mathrm{Reg}\overline{\psi}(k_{0t}\rho_{n,l}, \phi_{n,l})\right]_m = J_m(k_{0t}\rho_{n,l}) e^{-im\phi_{n,l}} \tag{15}$$

where Reg stands for the regular part. In order to apply the matrix formulation for the considered problem, one would require the isolated transition matrix of scatterers relating the amplitude of scattered field to the amplitude of incident field. This can be built using the solution obtained by Wait [16] for the Mie-type scattering coefficients of an isolated fiber. For an isolated scattered with the radius a, relative permittivity of ε_r and relative permeability of μ_r, we have:

$$\begin{bmatrix} b^{(s),EE} & b^{(s),EH} \\ c^{(s),HE} & c^{(s),HH} \end{bmatrix} = \overline{\overline{T}} \begin{bmatrix} a^{(i),E} \\ a^{(i),H} \end{bmatrix} = \begin{bmatrix} \overline{\overline{T}}_{11} & \overline{\overline{T}}_{12} \\ \overline{\overline{T}}_{21} & \overline{\overline{T}}_{22} \end{bmatrix} \begin{bmatrix} a^{(i),E} \\ a^{(i),H} \end{bmatrix} \tag{16}$$

$$\left[\overline{\overline{T_{11}}}\right]_m = \left[-\frac{J_m(v)}{H_m^{(1)}(v)} + \frac{2i\left(\frac{H_m^{(1)'}(v)}{vH_m^{(1)}(v)} - \frac{\mu_r J'_m(u)}{uJ_m(u)}\right)}{\pi v^2\left[H_m^{(1)}(v)\right]^2 D_m}\right] \tag{17}$$

$$\left[\overline{\overline{T_{12}}}\right]_m = \frac{k_0}{\mu_0\omega}\left[\frac{2}{\pi v^2}\left(\frac{1}{u^2} - \frac{1}{v^2}\right)\frac{mk_{0z}}{k_0\left[H_m^{(2)}(v)\right]^2 D_m}\right] \tag{18}$$

$$\left[\overline{\overline{T_{21}}}\right]_m = -\frac{k_0}{\varepsilon_0\omega}\left[\frac{2}{\pi v^2}\left(\frac{1}{u^2} - \frac{1}{v^2}\right)\frac{mk_{0z}}{k_0\left[H_m^{(2)}(v)\right]^2 D_m}\right] \tag{19}$$

$$\left[\overline{\overline{T_{22}}}\right]_m = \left[-\frac{J_m(v)}{H_m^{(1)}(v)} + \frac{2i\left(\frac{H_m^{(1)'}(v)}{vH_m^{(1)}(v)} - \frac{\varepsilon_r J'_m(u)}{uJ_m(u)}\right)}{\pi v^2\left[H_m^{(1)}(v)\right]^2 D_m}\right] \tag{20}$$

in which

$$u = \sqrt{\varepsilon_r\mu_r k_0^2 - k_{0z}^2}a \tag{21}$$

$$v = k_{0t}a \tag{22}$$

$$D_m = \left(\frac{H_m^{(1)'}(v)}{vH_m^{(1)}(v)} - \frac{\mu_r J'_m(u)}{uJ_m(u)}\right)\left(\frac{H_m^{(1)'}(v)}{vH_m^{(1)}(v)} - \frac{\varepsilon_r J'_m(u)}{uJ_m(u)}\right) - \frac{k_{0z}^2}{k_0^2}\left(\frac{1}{v^2} - \frac{1}{u^2}\right)^2 m^2 \tag{23}$$

Furthermore, the coefficient can be obtained for a coated fiber as well, which offers a great advantage as the computational complexity of the problem remains in the same order as a uniform fiber, while the other computational techniques may require a finer mesh to accurately reconstruct the structure. These coefficients are obtained by using the solutions of Shah [17]. Denoting the core and shell parameters by $a, \varepsilon_{r_1}, \mu_{r_1}$ and $b, \varepsilon_{r_2}, \mu_{r_2}$, respectively, we have:

$$\left[\overline{\overline{T_{11}}}\right]_m = \frac{|\delta_{11}|_m}{|\delta|_m} \tag{24}$$

$$\left[\overline{\overline{T_{12}}}\right]_m = \frac{|\delta_{12}|_m}{|\delta|_m} \tag{25}$$

$$\left[\overline{\overline{T_{21}}}\right]_m = \frac{|\delta_{21}|_m}{|\delta|_m} \tag{26}$$

$$\left[\overline{\overline{T_{22}}}\right]_m = \frac{|\delta_{22}|_m}{|\delta|_m} \tag{27}$$

where:

$$\delta = \begin{bmatrix} fH_n^{(1)'}(fb) & -f_1H_n^{(1)'}(f_1b) & f_1J_n'(f_1b) & 0 \\ 0 & f_1H_n^{(1)'}(f_1a) & -f_1J_n'(f_1a) & f_2J_n'(f_2a) \\ 0 & 0 & 0 & 0 \\ 0 & 0 & 0 & 0 \\ -\frac{inh}{kb}H_n^{(1)}(fb) & \frac{inh}{kb}H_n^{(1)}(f_1b) & -\frac{inh}{kb}J_n(f_1b) & 0 \\ 0 & -\frac{inh}{ka}H_n^{(1)}(f_1a) & \frac{inh}{ka}J_n(f_1a) & -\frac{inh}{ka}J_n(f_2a) \\ f^2H_n^{(1)}(fb) & -f_1^2H_n^{(1)}(f_1b) & f_1^2J_n(f_1b) & 0 \\ 0 & f_1^2H_n^{(1)}(f_1a) & -f_1^2J_n(f_1a) & f_2^2J_n(f_2a) \end{bmatrix}$$
$$\begin{bmatrix} \frac{inh}{kb}H_n^{(1)}(fb) & -\frac{inh}{m_1kb}H_n^{(1)}(f_1b) & \frac{inh}{m_1kb}J_n(f_1b) & 0 \\ 0 & -\frac{inh}{m_1ka}H_n^{(1)}(f_1a) & \frac{inh}{m_1ka}J_n(f_1a) & \frac{inh}{m_2ka}J_n(f_2a) \\ f^2H_n^{(1)}(fb) & -\frac{f_1^2}{m_1}H_n^{(1)}(f_1b) & \frac{f_1^2}{m_1}J_n(f_1b) & 0 \\ 0 & \frac{f_1^2}{m_1}H_n^{(1)}(f_1a) & -\frac{f_1^2}{m_1}J_n(f_1a) & \frac{f_2^2}{m_2}J_n(f_2a) \\ fH_n'(fb) & -m_1f_1H_n'(f_1b) & m_1f_1J_n'(f_1b) & 0 \\ 0 & m_1f_1H_n'(f_1a) & -m_1f_1J_n'(f_1a) & m_2f_2J_n'(f_2a) \\ 0 & 0 & 0 & 0 \\ 0 & 0 & 0 & 0 \end{bmatrix} \tag{28}$$

where $h = k_{0t}$, $f = k_{0z}$, $f_1 = \sqrt{\varepsilon_{r_1}\mu_{r_1}k_0^2 - k_{0z}^2}$, $f_2 = \sqrt{\varepsilon_{r_2}\mu_{r_2}k_0^2 - k_{0z}^2}$. δ_{11} and δ_{21} can be obtained by replacing the following vector with the first and fifth columns of δ, respectively.

$$a = \begin{bmatrix} \frac{inh}{kb}J_n(fb) & 0 & f^2J_n(fb) & 0 & fJ_n'(fb) & 0 & 0 & 0 \end{bmatrix} \tag{29}$$

Similarly, δ_{12} and δ_{22} can be obtained by replacing the following vector with the first and fifth columns of δ, respectively.

$$b = \begin{bmatrix} fJ_n'(fb) & 0 & 0 & 0 & \frac{inh}{kb}J_n(fb) & 0 & f^2J_n(fb) & 0 \end{bmatrix} \tag{30}$$

Having built the transition matrix of each scatterer, we can write the z component of the total fields outside the l-th scatterer in terms of basis column vectors in the l-th local coordinate system as:

$$\begin{aligned} \begin{bmatrix} E^{(tot)}(\rho_{0,l},\phi_{0,l}) \\ H^{(tot)}(\rho_{0,l},\phi_{0,l}) \end{bmatrix} &= \begin{bmatrix} E^{(i),\mathrm{TM}}(\rho_{0,l},\phi_{0,l}) \\ H^{(i),\mathrm{TE}}(\rho_{0,l},\phi_{0,l}) \end{bmatrix} + \sum_{i=1}^{N}\sum_{j=-\infty}^{+\infty} \begin{bmatrix} E_{j,i}^{(s)}(\rho_{0,l},\phi_{0,l}) \\ H_{j,i}^{(s)}(\rho_{0,l},\phi_{0,l}) \end{bmatrix} \\ &= \left(\begin{bmatrix} a^{(i),p,l} \\ a^{(i),s,l} \end{bmatrix} + \sum_{\substack{i=1 \\ i\neq l}}^{N}\sum_{j=-\infty}^{+\infty} \begin{bmatrix} a^{(s),p,i} \\ a^{(s),s,i} \end{bmatrix} \begin{bmatrix} \alpha_{ji,0l} & 0 \\ 0 & \alpha_{ji,0l} \end{bmatrix} \right) \begin{bmatrix} \mathrm{Re}\psi(k_{0t}\rho_l) \\ \mathrm{Re}\psi(k_{0t}\rho_l) \end{bmatrix} \\ &\quad + \begin{bmatrix} a^{(s),p,l} \\ a^{(s),s,l} \end{bmatrix} \begin{bmatrix} \psi(k_{0t}\rho_l) \\ \psi(k_{0t}\rho_l) \end{bmatrix} \end{aligned} \tag{31}$$

where $\alpha_{ji,0l}$ is the translation matrix, which relates the scattered harmonics at i-th local coordinate system inside the j-th unit-cell to the l-th local coordinate system inside 0-th unit-cell. The expression of such matrix is given by:

$$[\alpha_{ji,0l}]_{n,m} = H_{n-m}^{(1)}(k_{0t}d_{ji,0l})\exp(i(n-m)\phi_{ji,0l} - i(jk_{0x}\Lambda)) \tag{32}$$

where $d_{ji,0l} = \sqrt{(x_l - x_i - j\Lambda)^2 + (y_l - y_i)^2}$ and $\phi_{ji,0l} = \text{atan2}(y_l - y_i, x_l - x_i - j\Lambda)$.

In Eq. (31), the first term can be regarded as the incident field on the l-th isolated scatterer and the last term can be viewed as the scattered field. According to the definition of transition matrix, we can write:

$$\begin{bmatrix} a^{(s),p,l} \\ a^{(s),s,l} \end{bmatrix} = \overline{\overline{T_l}} \left(\begin{bmatrix} a^{(i),p,l} \\ a^{(i),s,l} \end{bmatrix} + \sum_{\substack{i=1 \\ i\neq l}}^{N} \sum_{j=-\infty}^{+\infty} \begin{bmatrix} a^{(s),p,i} \\ a^{(s),s,i} \end{bmatrix} \begin{bmatrix} \alpha_{ji,0l} & 0 \\ 0 & \alpha_{ji,0l} \end{bmatrix} \right) \tag{33}$$

which can be rewritten as:

$$\left(\overline{\overline{T_l}}\right)^{-1} \begin{bmatrix} a^{(s),p,l} \\ a^{(s),s,l} \end{bmatrix} - \sum_{i=1}^{N} \begin{bmatrix} a^{(s),p,i} \\ a^{(s),s,i} \end{bmatrix} \begin{bmatrix} \sum\limits_{j=-\infty}^{+\infty} \alpha_{ji,0l} & 0 \\ 0 & \sum\limits_{j=-\infty}^{+\infty} \alpha_{ji,0l} \end{bmatrix} = \begin{bmatrix} a^{(i),p,l} \\ a^{(i),s,l} \end{bmatrix} \tag{34}$$

Writing this coupling equation for all the cylinders inside the unit-cell, we arrive at a system of N linear equations the solution of which gives us the unknown scattered field coefficients.

2.3. Evaluation of Lattice Sums

One of the challenges faced by multipole methods in solving periodic structures is the calculation of highly oscillating and slowly convergent lattice sums involving the translation of harmonics. These summations do not have a closed-form response except for on-axis periodicity that is when all the fibers are located on the x axis. One of the ways to avoid this challenge, which has been previously used for the 2D case and T-matrix method is to translate all the harmonics into the center and build the aggregate T-matrix [33, 35]. However, this approach might fail when the fiber separation distance within the unit-cell is large, as it gives rise to ill-conditioned matrices, which will break down the solution of matrix equation. Moreover, the information regarding the coupling of the elements in the near-field will be lost in this approach. For the general case, a robust approach is required for calculation of infinite summations in the forms of:

$$S = \lim_{k\to\infty} S_k = \lim_{k\to\infty} \sum_{j=-k}^{+k} \alpha_{ji,0l} = \lim_{k\to\infty} \sum_{j=-k}^{+k} H^{(1)}_{n-m}(k_{0t} d_{ji,0l}) \exp(i(n-m)\phi_{ji,0l} - i(jk_{0x}\Lambda)) \tag{35}$$

For this purpose, we have adopted an adaptive mathematical algorithm based on Shank's transformation to calculate the infinite series. The Shanks' sequence transformation [42] $e_p : (S_k) \mapsto \{e_p(S_k)\}$ consists of transforming a given sequence (S_k) into the set of sequences $e_p(S_k)$ whose terms are defined by:

$$e_p(S_k) = \frac{\mathrm{H}_{p+1}(S_k)}{\mathrm{H}_p(\Delta^2 S_k)}, \quad p, k = 0, 1, \ldots \tag{36}$$

where Δ is the forward operator and H_k is the Hankel determinant [42].

The ε-algorithm is a recursive algorithm due to Wynn [43] for implementing the Shanks' transformation without computing the Hankel determinants appearing in (36). The ε-algorithm is recommended as the best all-purpose acceleration method for slowly converging sequences and consists of replacing the sequence S_k with the sequence ε_0^k, which is defined by the following non-linear recurrence relation:

$$\varepsilon_{p+1}^{(k)} = \varepsilon_{p-1}^{(k+1)} + \left[\varepsilon_p^{(k+1)} - \varepsilon_p^{(k)}\right]^{-1}, \quad k, p = 0, 1, \ldots \tag{37}$$

with

$$\varepsilon_k^{(-1)} = 0, \quad \varepsilon_k^{(0)} = S_k, \tag{38}$$

For higher-order multipoles, the convergence is slower. In order to improve the performance, we implement an adaptive multistep algorithm [44]. The recursive rule in this case is defined for the m-th step as:

$$\varepsilon_{p+1,m}^{(k)} = \varepsilon_{p-m,m}^{(k+1)} + \Pi_{i=1}^{m} \left[\varepsilon_{p-m+i,m}^{(k+1)} - \varepsilon_{p-m+i,m}^{(k)}\right]^{-1}, \quad k, p = 0, 1, \ldots \tag{39}$$

In order to ensure convergence, an adaptive approach is used. The number of sampling points and extrapolation steps are increased at each iteration, until the results are converged by a predefined threshold. The same approach is used for evaluation of the near-field expressions given by Equations (12) and (13).

2.4. Bi-Periodic Gratings and Scattering Matrix

Figure 4(a) shows a schematic of the unit-cell of a fabric structure given as a bi-periodic grating of fibers crossed at the right angle. This problem is essentially a 3D problem, which poses computational challenges for any numerical method, as discussed in the introduction. Here, we demonstrate a 2D treatment of such a 3D problem. This is done by making use of the scattering matrix approach to handle coupling between the crossed grating layers in the Cartesian coordinates through recursive formulae. In order to make all the reflection and transmission coefficients unit-less we scale the magnetic field by the wave impedance of free-space $\tilde{H}_z = \eta_0 H_z$.

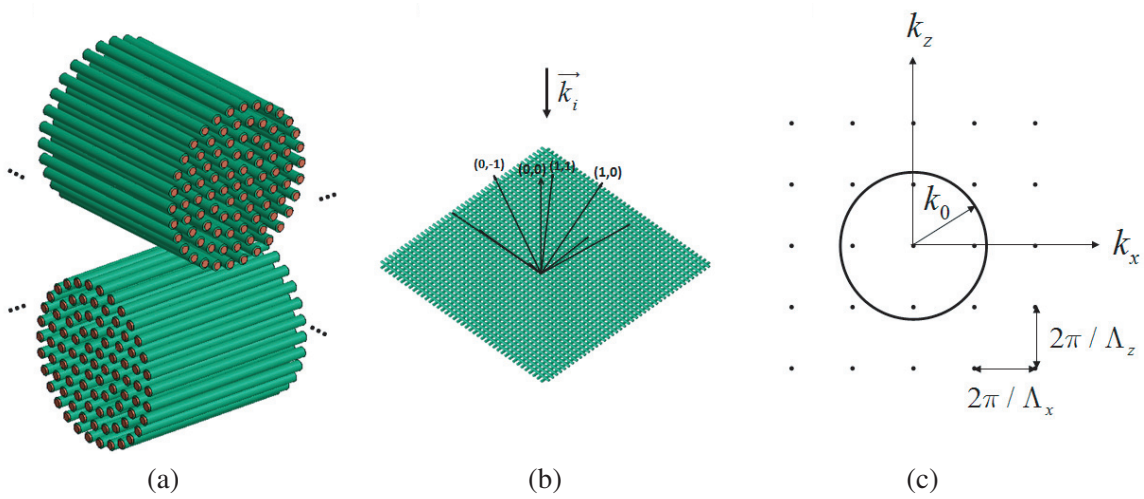

Figure 4. (a) The 3D unit-cell of a fabric structure given as a stack of crossed grating layers, (b) schematic representation of diffraction orders from the bi-periodic fabric structure, (c) accessible diffraction modes with a bi-periodic grating, represented in wavevector space.

We define the scattering matrix as:

$$\begin{pmatrix} E_z^{(d)-} \\ \tilde{H}_z^{(d)-} \\ E_z^{(d)+} \\ \tilde{H}_z^{(d)+} \end{pmatrix} = \overline{\overline{S}} \begin{pmatrix} E_z^{(i)+} \\ \tilde{H}_z^{(i)+} \\ E_z^{(i)-} \\ \tilde{H}_z^{(i)-} \end{pmatrix} \tag{40}$$

where $+$ and $-$ denote fields propagating upwards and downwards, respectively. Superscripts (d) and (i) denote the diffracted and incident fields, respectively. Treating each grating layer as an interface, the scattering matrix of each interface can be expressed as:

$$\overline{\overline{S}} = \begin{pmatrix} R^+ & T^- \\ T^+ & R^- \end{pmatrix} = \begin{pmatrix} r_{pp}^+ & r_{ps}^+ & t_{pp}^- & t_{ps}^- \\ r_{sp}^+ & r_{ss}^+ & t_{sp}^- & t_{ss}^- \\ t_{pp}^+ & t_{ps}^+ & r_{pp}^- & r_{ps}^- \\ t_{sp}^+ & t_{ss}^+ & r_{sp}^- & r_{ss}^- \end{pmatrix} \tag{41}$$

where the subscript s represents the transverse electric component of waves and p represents the transverse magnetic component of waves. The periodicity of the fabric structure in x and z directions

gives rise to a group of diffracted plane waves as shown in Fig. 4(b) whose x and z dependencies are given by $\exp(ik_{x,p}x)$ and $\exp(ik_{z,q}z)$, respectively, where

$$k_{x,p} = k_{0x} + \frac{2\pi p}{\Lambda_x} \tag{42}$$

$$k_{z,q} = k_{0z} + \frac{2\pi q}{\Lambda_z} \tag{43}$$

where Λ_x and Λ_z are the periodicities in x- and z-directions, respectively. Each pair (p, q), thus, specifies a diffracted plane-wave order and, for notational convenience, we map each (p, q) to a unique integer v, and use the subscript v to denote quantities associated with the (p, q)-th order. Note that the v-th plane-wave order is propagating if

$$k_{yv}^2 = k_0^2 - k_{x,p}^2 - k_{y,q}^2 \tag{44}$$

The accessible diffraction modes with a bi-periodic grating are represented in wavevector space in Fig. 4(c). The propagating modes are the ones inside the circle with a radius of k_0. Fixing the values of p and q and then projecting the problem onto the x-z plane allows us to use the multipole method to solve for the part of the diffracted field having an x dependence of $\exp(ik_{x,p}x)$ and z dependence of $\exp(ik_{z,q}z)$ for each layer of the grating.

While the plane wave diffraction problem is best formulated in terms of parallel/perpendicular (p/s) polarizations, the multipole scattering problem is best handled in terms of TM/TE modes with respect to the principal Cartesian field components parallel to the cylinder axes. This requires translation of reflection and transmission coefficient from the TM/TE modes to p/s polarizations. For this purpose, we have [26, 40]:

$$\begin{bmatrix} r_{pp}^{\pm} & r_{ps}^{\pm} \\ r_{sp}^{\pm} & r_{ss}^{\pm} \end{bmatrix} = \left(\chi^{\pm}\right)^{-1} \begin{bmatrix} r_{\mathrm{TM/TM}}^{\pm} & r_{\mathrm{TM/TE}}^{\pm} \\ r_{\mathrm{TE/TM}}^{\pm} & r_{\mathrm{TE/TE}}^{\pm} \end{bmatrix} \chi^{\pm} \tag{45}$$

where

$$\chi^{\pm} = \begin{bmatrix} -\xi_\beta & \xi_\alpha \\ \mp\xi_\alpha & \mp\xi_\beta \end{bmatrix} \tag{46}$$

in which

$$\xi_\beta = \left[(k_{yv}/k_0)^{-1/2} k_{x,p}/\sqrt{k_{x,p}^2 + k_{z,q}^2}\right] \tag{47}$$

$$\xi_\alpha = \left[(k_{yv}/k_0)^{1/2} k_{z,q}/\sqrt{k_{x,p}^2 + k_{z,q}^2}\right] \tag{48}$$

To derive the reflection and transmission coefficients of the array, we consider TM and TE polarizations separately. Equations (12)–(13) are then rewritten in terms of the Floquet modes. Using the recurrence formula and Fourier integral representation of Hankel functions, considering $k_{yv} < 0$, the reflected fields $E_z^{(d)+}, \tilde{H}_z^{(d)+}$ in $y > 0$ domain and the transmitted field $E_z^{(d)-}, \tilde{H}_z^{(d)-}$ in $y < 0$ domain are obtained as follows [33, 35]:

For the TM polarization:

$$E^{(d)+} = \sum_{v=-\infty}^{+\infty} \sum_{i=1}^{N} p_{v,i}^T \cdot b^{(s),EE,i} \exp\left[i(k_{0x}x + k_{0y}y + k_{0z}z)\right] \tag{49}$$

$$E^{(d)-} = \sum_{v=-\infty}^{+\infty} \sum_{i=1}^{N} \left(q_{v,i}^T \cdot b^{(s),EE,i} + \delta_{v0}\right) \exp\left[i(k_{0x}x - k_{0y}y + k_{0z}z)\right] \tag{50}$$

$$\tilde{H}^{(d)+} = \sum_{v=-\infty}^{+\infty} \sum_{i=1}^{N} p_{v,i}^T \cdot c^{(s),HE,i} \exp\left[i(k_{0x}x + k_{0y}y + k_{0z}z)\right] \tag{51}$$

$$\tilde{H}^{(d)-} = \sum_{v=-\infty}^{+\infty} \sum_{i=1}^{N} q_{v,i}^T \cdot c^{(s),HE,i} \exp\left[i(k_{0x}x - k_{0y}y + k_{0z}z)\right] \tag{52}$$

where:

$$p_{v,i} = \begin{bmatrix} \dfrac{2(-i)^m(k_{xv}+ik_{yv})^m}{\Lambda k_{yv}k_0^m}\exp\left[i(k_{xv}x_i+k_{yv}y_i)\right] & m\geq 0 \\ \dfrac{2i^{|m|}(k_{xv}-ik_{yv})^{|m|}}{\Lambda k_{yv}k_0^{|m|}}\exp\left[i(k_{xv}x_i+k_{yv}y_i)\right] & m<0 \end{bmatrix} \tag{53}$$

$$q_{v,i} = \begin{bmatrix} \dfrac{2(-i)^m(k_{xv}-ik_{yv})^m}{\Lambda k_{yv}k_0^m}\exp\left[i(k_{xv}x_i+k_{yv}y_i)\right] & m\geq 0 \\ \dfrac{2i^{|m|}(k_{xv}+ik_{yv})^{|m|}}{\Lambda k_{yv}k_0^{|m|}}\exp\left[i(k_{xv}x_i+k_{yv}y_i)\right] & m<0 \end{bmatrix} \tag{54}$$

Thus, we can obtain:

$$r^+_{\mathrm{TM/TM},v} = \sum_{i=1}^{N} p^T_{v,i}\cdot b^{(s),EE,i} \tag{55}$$

$$t^-_{\mathrm{TM/TM},v} = \sum_{i=1}^{N}\left(q^T_{v,i}\cdot b^{(s),EE,i}+\delta_{v0}\right) \tag{56}$$

$$r^+_{\mathrm{TE/TM},v} = \sum_{i=1}^{N} p^T_{v,i}\cdot c^{(s),HE,i} \tag{57}$$

$$t^-_{\mathrm{TE/TM},v} = \sum_{i=1}^{N} q^T_{v,i}\cdot c^{(s),HE,i} \tag{58}$$

Similarly, the TE polarization results into:

$$r^+_{\mathrm{TE/TE},v} = \sum_{i=1}^{N} p^T_{v,i}\cdot c^{(s),HH,i} \tag{59}$$

$$t^-_{\mathrm{TE/TE},v} = \sum_{i=1}^{N}\left(q^T_{v,i}\cdot c^{(s),HH,i}+\delta_{v0}\right) \tag{60}$$

$$r^+_{\mathrm{TM/TE},v} = \sum_{i=1}^{N} p^T_{v,i}\cdot b^{(s),EH,i} \tag{61}$$

$$t^-_{\mathrm{TM/TE},v} = \sum_{i=1}^{N} q^T_{v,i}\cdot b^{(s),EH,i} \tag{62}$$

The coefficients t_v^+ and r_v^- will be obtained in a similar way, considering $k_{yv}>0$. Obviously, if the unit-cells are symmetric with respect to array plane we have $R^+=R^-$ and $T^+=T^-$. The scattering matrix of each layer can be built by the aforementioned procedure. In case that the layers are the same except for the orientation, the scattering matrix of the crossed layer can be built by properly permuting the scattering matrix of the other layer such that $k'_{x,p}=k_{y,p}$ and $k'_{y,q}=-k_{x,-q}$.

Then, the overall reflection and transmission coefficients can be obtained using recurrence relationships for the scattering matrices for a stack of $s+1$ non-interpenetrating gratings [41]:

$$R^{+,s+1} = R^+ + T^-PR^{+,s}P\left(I-R^-PR^{+,s}P\right)^{-1}T^+ \tag{63}$$

$$R^{-,s+1} = R^{-,s} + T^{+,s}PR^-P\left(I-R^{+,s}PR^-P\right)^{-1}T^{-,s} \tag{64}$$

$$T^{+,s+1} = T^{+,s}P\left(I-R^-PR^{+,s}P\right)^{-1}T^+ \tag{65}$$

$$T^{-,s+1} = T^-P\left(I-R^{+,s}PR^-P\right)^{-1}T^{-,s} \tag{66}$$

where I is the identity matrix and P is the matrix accounting for the change in phase that occurs for fields propagating between successive layers and is defined as:

$$P = \begin{bmatrix} \exp(ik_{yv}h) & 0 \\ 0 & \exp(ik_{yv}h) \end{bmatrix} \tag{67}$$

in which h is the distance between interfaces s and $s+1$. Obviously, the formulation holds true for an arbitrary number of grating layers as well as in the presence of any substrate/superstrate medium.

The diffraction efficiencies can be obtained:

$$\mathrm{R}_v^{pp,sp,ps,sp} = \frac{\mathrm{Re}\{k_{yv}\}}{k_{y0}} \left(|r_v^{pp,sp,ps,sp}|^2\right) \tag{68}$$

According to the law of conservation of energy, for a structure made of lossless materials:

$$\sum_v \mathrm{R}_v^{pp} + \mathrm{R}_v^{ps} + \mathrm{T}_v^{pp} + \mathrm{T}_v^{ps} = 1 \tag{69}$$

$$\sum_v \mathrm{R}_v^{ss} + \mathrm{R}_v^{sp} + \mathrm{T}_v^{ss} + \mathrm{T}_v^{sp} = 1 \tag{70}$$

Finally, in order to be able to plot the near-fields we need to obtain the fields inside the grating layers, as the Fourier integral representations of the fields are only valid outside the grating layers. For this purpose, after obtaining all the forward and backward waves above and below the grating layers, we use the waves propagating towards each interface as input of the multipole expansion method and obtain the scattering coefficients of the cylinders. The field inside the grating layers can then be evaluated through Equations (12)–(13). According to the Floquet theorem, the outgoing waves from the interfaces will be the continuation of the obtained fields outside the grating.

3. NUMERICAL RESULTS AND DISCUSSION

In this section, sample numerical results are presented to evaluate the validity and efficiency of the developed formulation for modeling large-scale fabric structures. All the simulations are performed on a Linux-based machine with Intel Xeon(R) CPU E5-2670 v3 @ 2.30 GHz and 11.5 GB RAM. For the FDTD simulations NVIDIA®Tesla®K40C GPU accelerator was utilized.

In our simulations, the number of multipoles are truncated to $M = \mathrm{round}(3k_0\sqrt{\varepsilon_r\mu_r}a)$ [20, 21]. In order to ensure convergence, we have considered $-10 \leq p, q \leq 10$ which is equivalent to 21 diffraction orders for 1D periodicity and 441 diffraction orders for 2D periodicity. Lattice sums are evaluated using an adaptive criterion with the prescribed accuracy of 10^{-6}. The near-field summations are evaluated using 19 sample points and 8 steps in the multi-step Wynn algorithm. A great accuracy is afforded using these parameters.

First, we consider circular arrays of coated fibers arranged into collective bundles representing the formation of yarns to validate our matrix formulation for periodic arrangements. The yarns are positioned in a periodic staggered configuration oriented 30 degrees relative to the horizontal plane as shown in Fig. 5(a). Such geometry can be regarded as a 2D model of a woven fabric [1]. The parameters include: $D_f = 1\,\mu\mathrm{m}$ — the fiber diameter, $D_{core} = 0.5\,\mu\mathrm{m}$ — the core diameter, $\varepsilon_{shell} = 2.25$ — the shell relative permittivity, $\varepsilon_{core} = 6.25$ — the core relative permittivity, $D_y = 30\,\mu\mathrm{m}$ — the yarn diameter, $D_s = 1\,\mu\mathrm{m}$ — the edge-to-edge fiber separation distance, and $D_p = 6\,\mu\mathrm{m}$ — the edge-to-edge yarn separation distance. The total number of fibers within a yarn is 169 and the periodicity is 60.6 µm. The structure is illuminated by a normal TM^z plane wave with the wavelength of $\lambda = 15\,\mu\mathrm{m}$.

The normal component of the electric field, E_z, is obtained using the proposed method and compared with FDTD results. The near-fields are plotted in Fig. 5. A great agreement is observed between the results which verifies the validity of our method.

The computational time and memory requirements for the methods, corresponding to the solution of the considered structure are compared in Table 1. A cell size of 50 nm is used for FDTD discretization to minimize the shape reconstruction errors and ensure the convergence. The grid size is $1633\times1318\times11$ and the number of time steps is 9000. Periodic boundary conditions are applied along x and z directions and the domain is terminated by perfectly matched layer in the y direction. As can be seen, a significant

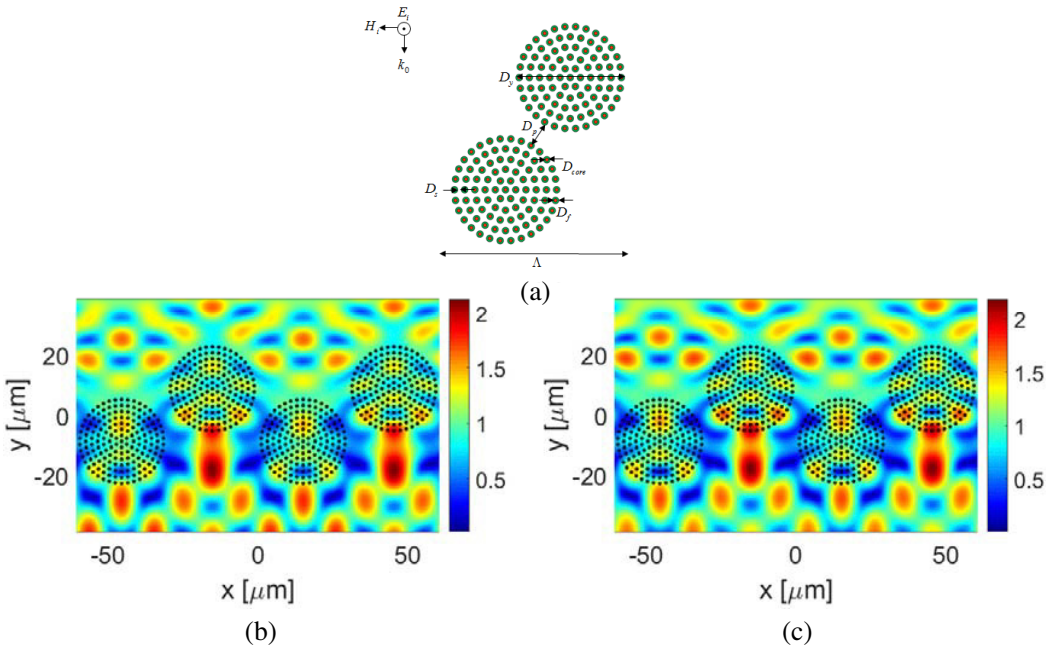

Figure 5. (a) A schematic of the 2D unit-cell simulated here representing a 2D model of woven fabric consisted of coated fibers arranged in circular yarns. (b) and (c) Correspond to the near-field distribution of the normal component of the electric field obtained with the proposed and FDTD methods, respectively.

Table 1. Comparison of the memory requirement and computation time between the proposed method and FDTD for the fabric structure given in Fig. 5(a).

	Proposed Method on CPU	FDTD on High-Performance GPU
Number of Unknowns	845	$\sim 1.42 \times 10^8$
Memory Requirement	12 MB	2.7 GB
Computation Time	$\sim$ 30 seconds	$\sim$ 28.5 minutes

computational gain is achieved by the proposed method. The memory requirement is decreased by a factor of 225 and the computation time is reduced by a factor of 57. We need to remind that the FDTD analysis is suited and performed on a GPU based machine and it will take much longer if one simulates on the same machine as for our proposed model ($\sim$ 7 hours).

Next, we apply the method to model a practical large-scale bi-periodic fabric structure. The structure is consisted of a crossed pair of non-interlaced yarns (weft and wraps). Each yarn is a circular array of fibers. The parameters are chosen as $D_f = 2\,\mu$m — the fiber diameter, $\varepsilon_{fiber} = 2.25$ — the fiber relative permittivity, $D_y = 30\,\mu$m — the yarn diameter, $D_s = 1\,\mu$m — the edge-to-edge fiber separation distance, and $D_p = 5\,\mu$m — the edge-to-edge yarn separation distance. The total number of fibers within a yarn is 91 and the period is 35 μm. The structure is illuminated by a normal TM^z plane wave with the wavelength of $\lambda = 15\,\mu$m. Fig. 6 compares the results of the proposed method and FDTD for the near-field distribution of the normal component of the electric field. It should be remarked that here, we calculate the fields outside the grating layers using the scattering matrix approach and the fields inside the gratings are obtained by reusing the multipole expansion method for each layer and considering amplitudes of the waves propagating towards each interface as the excitations. As it can be seen, the continuity of E_z component in the TM^z excitation is satisfied with a great accuracy. Moreover, a remarkable consistency is observed between the results by the proposed method and those of FDTD.

The computational time and memory requirements for the methods corresponding to the 3D unit-cell simulation are compared in Table 2. Here, a mesh size of $\Delta = 100\,$nm is used for FDTD

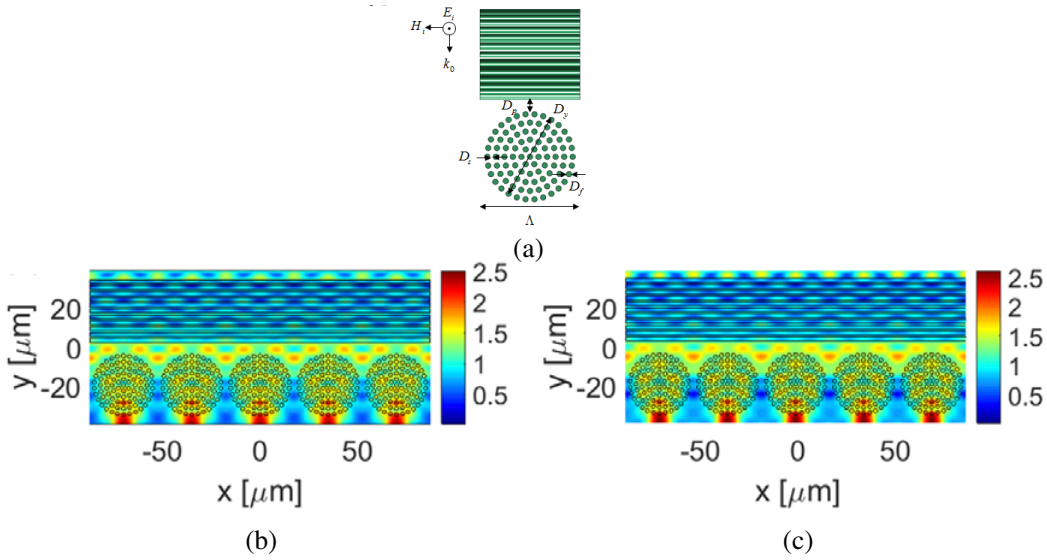

Figure 6. (a) A schematic of the 3D unit-cell simulated here representing a 3D model of non-interlaced fabric structure consisted of crossed gratings of fibers arranged in circular yarns (weft and wrap). (b) and (c) Correspond to the near-field distribution of the normal component of the electric field obtained with the proposed and FDTD methods, respectively.

Table 2. Comparison of the memory requirement and computation time between the proposed method and FDTD for the fabric structure given in Fig. 6(a).

	Proposed Method on CPU	FDTD on High-Performance GPU
Number of Unknowns	910	$\sim 5.96 \times 10^8$
Memory Requirement	15 MB	10.5 GB
Computation Time	~ 5 min	~ 14.4 hours

discretization (a finer mesh could not be used with the available computational resources). The grid size is $812 \times 350 \times 350$ and the number of time steps is 8160. It should be remarked that the unit cell of such structure is $2.4\lambda \times 2.4\lambda \times 4.4\lambda$ which considering the fine meshing one would need to minimize the shape reconstruction errors and to reach convergence, it poses a great challenge for FDTD. The computational gain obtained in this case is even more pronounced comparing to the 2D case; the computational time is reduced by a factor 172 and the memory requirement is decreased by a factor of 700. This is due to the semi-3D nature of our formulation which allows for the 2D treatment of the complex 3D geometry so that the computations can be done with the same order of complexity as the 2D problem.

It should be taken into consideration in the above comparisons that FDTD is a time-domain technique, and when a broadband pulse is used as the source, then the response over a wide range of frequencies can be obtained with a single simulation while for the frequency-domain techniques such as ours the simulations need to be repeated for each single frequency. However, given the statistics of our model one can see significant benefit even if a broadband result is desired. Moreover, it does not require expensive post-processing to obtain diffraction efficiencies. Transmittance, reflectance and absorptance of the considered 3D fabric structure over the thermal radiation spectrum are plotted in Fig. 7. The results are shown for TM-polarized and TE-polarized incidence as well as un-polarized incidence, given as average of TM and TE. Over this wide spectral range, the dimensions of the unit-cell vary from $7.2\lambda \times 7.2\lambda \times 13.2\lambda$ to $1.44\lambda \times 1.44\lambda \times 2.64\lambda$ and the number of propagating diffraction orders changes from 225 to 9. As it can be seen, the absorptance is less than 10^{-8} over the whole spectrum and the energy is conserved with a great accuracy, which is another testimony to the method's accuracy and

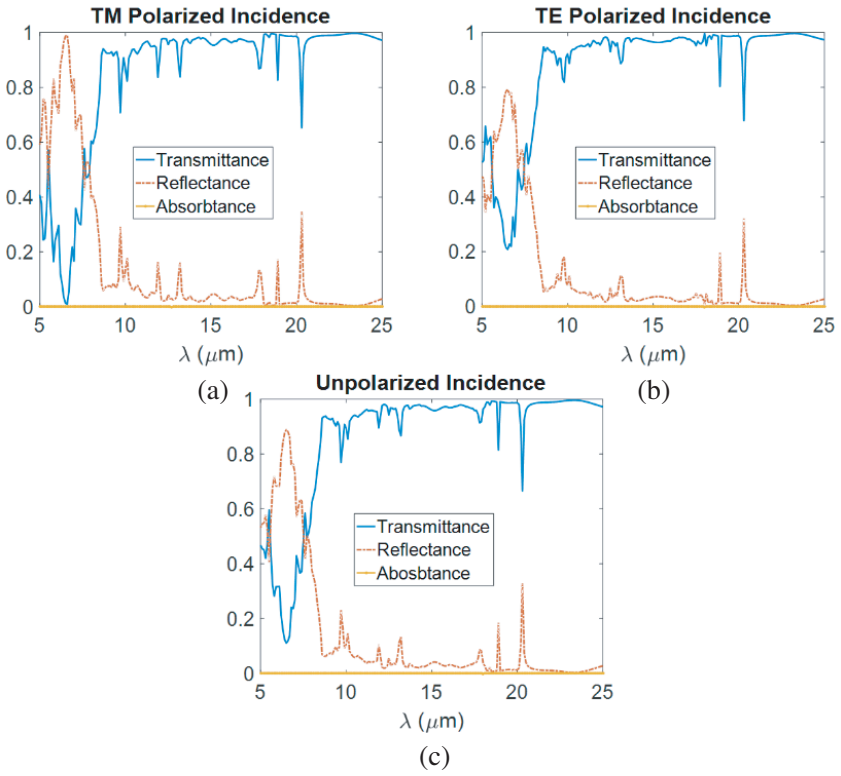

Figure 7. The transmittance, reflectance and absorptance spectra of the above-mentioned fabric structure for (a) TM polarized incidence, (b) TE polarized incidence and (c) un-polarized incidence.

validity. A step of 0.1 μm is used for sweeping the spectrum and the total computation time was around 1 hour which still outperforms brute force methods such as FDTD.

In the presented reflectance and transmittance spectra one can notice a drop in the level of transmittance at wavelengths lower than 9 μm. This is due to the increase in the number of induced cavity modes and confinement of the fields to the fibers as their effective size increase. This drop is more pronounced for the TM polarization, which shows the stronger interaction of fabric structure with TM mode. Another implication of this is the polarization sensitivity of fabric structures as opposed to the woodpile structures. Such studies provide important information regarding the thermal performance of fabric structures and are critical for designing fabrics and textiles with novel functionalities [1, 2].

4. CONCLUSION

We have developed a robust framework for analysis of electromagnetic scattering from fabric structures, modeled as crossed gratings of cylindrical fibers, arranged in arbitrary bundles (yarns). The proposed technique uses a rigorous matrix formulation for analysis of conical scattering from periodic arbitrary arrangement of coated fibers. The coupling between crossed gratings is treated using recursive formulae of scattering matrix. The method is applied to analyzing practical large-scale fabric structures and both near-field and far-field results are presented. The results are compared with full-wave simulation. A complete agreement is observed between the results, while a significant computational gain is afforded by the proposed method. The method can be used to model any arbitrary number of fabric layers embedded in any layered media. Moreover, it can handle any arbitrary arrangement of uniform fibers and core-shell fibers made of different materials with equal ease. Because of its generality and efficiency, it should be useful for the design and optimization of the performance of textiles and fabric structures for a variety of applications.

ACKNOWLEDGMENT

This work is supported by DARPA via Grant No. N00014-14-1-0850. The authors would like to also acknowledge several helpful discussions with Sandeep Inampudi.

REFERENCES

1. Tong, J. K., X. Huang, S. V. Boriskina, J. Loomis, Y. Xu, and G. Chen, "Infrared-transparent visible-opaque fabrics for wearable personal thermal management," *ACS Photonics*, Vol. 2, No. 6, 769–778, 2015, doi:10.1021/acsphotonics.5b00140.
2. Hsu, P.-C., X. Liu, C. Liu, X. Xie, H. R. Lee, A. J. Welch, T. Zhao, and Y. Cui, "Personal thermal management by metallic nanowire-coated textile," *Nano Letters*, Vol. 15, No. 1, 365–371, 2015, doi:10.1021/nl5036572.
3. Pan, S., Z. Yang, P. Chen, J. Deng, H. Li, and H. Peng, "Wearable solar cells by stacking textile electrodes," *Angewandte Chemie*, Vol. 126, No. 24, 6224–6228, 2014, doi:10.1002/ange.201402561.
4. Zhang, N., J. Chen, Y. Huang, W. Guo, J. Yang, J. Du, X. Fan, and C. Tao, "A wearable all-solid photovoltaic textile," *Advanced Materials*, Vol. 28, No. 2, 263–269, 2015, doi:10.1002/adma.201504137.
5. Zhang, Z., X. Chen, P. Chen, G. Guan, L. Qiu, H. Lin, Z. Yang, W. Bai, Y. Luo, and H. Peng, "Integrated polymer solar cell and electrochemical supercapacitor in a flexible and stable fiber format," *Advanced Materials*, Vol. 26, No. 3, 466–470, 2013, doi:10.1002/adma.201302951.
6. Zhang, Z., X. Li, G. Guan, S. Pan, Z. Zhu, D. Ren, and H. Peng, "A lightweight polymer solar cell textile that functions when illuminated from either side," *Angewandte Chemie*, Vol. 126, No. 43, 11755–11758, 2014, doi:10.1002/ange.201407688.
7. Erdumlu, N. and C. Saricam, "Electromagnetic shielding effectiveness of woven fabrics containing cotton/metal-wrapped hybrid yarns," *Journal of Industrial Textiles*, Vol. 46, No. 4, 1084–1103, 2015, doi:10.1177/1528083715613628.
8. Roh, J. S., Y. S. Chi, T. J. Kang, and S. W. Nam, "Electromagnetic shielding effectiveness of multifunctional metal composite fabrics," *Textile Research Journal*, Vol. 78, No. 9, 825–835, 2008, doi:10.1177/0040517507089748.
9. Narbonneau, F., D. Kinet, B. Paquet, A. Depré, J. de Jonckheere, R. Logier, J. Zinke, J. Witt, and K. Krebber, "Smart textile embedding optical fibre sensors for healthcare monitoring during MRI," *Advances in Science and Technology*, Vol. 60, 134–143, 2008, doi:10.4028/www.scientific.net/ast.60.134.
10. Ciocchetti, M., C. Massaroni, P. Saccomandi, M. Caponero, A. Polimadei, D. Formica, and E. Schena, "Smart textile based on fiber bragg grating sensors for respiratory monitoring: Design and preliminary trials," *Biosensors*, Vol. 5, No. 3, 602–615, 2015, doi:10.3390/bios5030602.
11. Boriskin, A. V., S. V. Boriskina, A. Rolland, R. Sauleau, and A. I. Nosich, "Test of the FDTD accuracy in the analysis of the scattering resonances associated with high-Q whispering-gallery modes of a circular cylinder," *Journal of the Optical Society of America A*, Vol. 25, No. 5, 1169, 2008, doi:10.1364/josaa.25.001169.
12. Jin, J.-M. and V. V. Liepa, "Application of hybrid finite element method to electromagnetic scattering from coated cylinders," *IEEE Transactions on Antennas and Propagation*, Vol. 36, No. 1, 50–54, 1988, doi:10.1109/8.1074.
13. Yashiro, K. and S. Ohkawa, "Boundary element method for electromagnetic scattering from cylinders," *IEEE Transactions on Antennas and Propagation*, Vol. 33, No. 4, 383–389, 1985, doi:10.1109/tap.1985.1143587.
14. Jarem, J. M., "rigorous coupled wave analysis of bipolar cylindrical systems: Scattering from inhomogeneous dielectric material, eccentric, composite circular cylinders," *Progress In Electromagnetics Research*, Vol. 43, 181–237, 2003, doi:10.2528/pier03042304.

15. Twersky, V., "Multiple scattering of radiation by an arbitrary planar configuration of parallel cylinders and by two parallel cylinders," *Journal of Applied Physics*, Vol. 23, No. 4, 407, 1952, doi:10.1063/1.1702220.
16. Wait, J. R., "Scattering of a plane wave from a circular dielectric cylinder at oblique incidence," *Canadian Journal of Physics*, Vol. 33, No. 5, 189–195, 1955, doi:10.1139/p55-024.
17. Shah, G. A., "scattering of plane electromagnetic waves by infinite concentric circular cylinders at oblique incidence," *Monthly Notices of the Royal Astronomical Society*, Vol. 148, No. 1, 93–102, 1970, doi:10.1093/mnras/148.1.93.
18. Lee, S.-C., "Scattering by closely-spaced radially-stratified parallel cylinders," *Journal of Quantitative Spectroscopy and Radiative Transfer*, Vol. 48, No. 2, 119–130, 1992, doi:10.1016/0022-4073(92)90081-e.
19. Felbacq, D., G. Tayeb, and D. Maystre, "Scattering by a random set of parallel cylinders," *Journal of the Optical Society of America A*, Vol. 11, No. 9, 2526, 1994, doi:10.1364/josaa.11.002526.
20. Henin, B. H., A. Z. Elsherbeni, and M. H. Al Sharkawy, "Oblique incidence plane wave scattering from an array of circular delectric cylinders," *Progress In Electromagnetics Research*, Vol. 68, 261–279, 2007, doi:10.2528/pier06083102.
21. Henin, B. H., M. H. Al Sharkawy, and A. Z. Elsherbeni, "Scattering of obliquely incident plane wave by an array of parallel concentric metamaterial cylinders," *Progress In Electromagnetics Research*, Vol. 77, 285–307, 2007, doi:10.2528/pier07082102.
22. Kiani, M., A. Abdolali, and M. M. Salary, "EM scattering from cylindrical structures coated by materials with inhomogeneity in both radial and azimuthal directions," *IEEE Transactions on Antennas and Propagation*, Vol. 63, No. 3, 1118–128, 2015, doi:10.1109/tap.2015.2391289.
23. Abdolali, A., M. Kiani, and M. M. Salary, "Numerical analysis of scattering from cylindrical structures coated by layers having inhomogeneity in both radial and azimuthal directions," *IET Microwaves, Antennas & Propagation*, Vol. 9, No. 5, 472–85, 2015, doi:10.1049/iet-map.2014.0135.
24. Wu, Y. and Y. Y. Lu, "Dirichlet-to-neumann map method for analyzing periodic arrays of cylinders with oblique incident waves," *Journal of the Optical Society of America B*, Vol. 26, No. 7, 1442, 2009, doi:10.1364/josab.26.001442.
25. Yuan, J. and Y. Y. Lu, "Photonic bandgap calculations with dirichlet-to-neumann maps," *Journal of the Optical Society of America A*, Vol. 23, No. 12, 3217, 2006, doi:10.1364/josaa.23.003217.
26. Smith, G. H., L. C. Botten, R. C. Mcphedran, and N. A. Nicorovici, "Cylinder gratings in conical incidence with applications to modes of air-cored photonic crystal fibers," *Physical Review E*, Vol. 66, No. 5, 2002, doi:10.1103/physreve.66.056604.
27. Waterman, P. C., "Matrix formulation of electromagnetic scattering," *Proceedings of the IEEE*, Vol. 53, No. 8, 805–12, 1965, doi:10.1109/proc.1965.4058.
28. Peterson, B. and S. Ström, "T matrix for electromagnetic scattering from an arbitrary number of scatterers and representations of E (3)," *Physical Review D*, Vol. 8, No. 10, 3661–678, 1973, doi:10.1103/physrevd.8.3661.
29. Peterson, B. and S. Ström, "T-matrix formulation of electromagnetic scattering from multilayered scatterers," *Physical Review D*, Vol. 10, No. 8, 2670–684, 1974, doi:10.1103/physrevd.10.2670.
30. Roussel, H., W. C. Chew, F. Jouvie, and W. Tabbara, "Electromagnetic scattering from dielectric and magnetic gratings of fibers — A T-matrix solution," *Journal of Electromagnetic Waves and Applications*, Vol. 10, No. 1, 109–127, 1996.
31. Chew, W. C., *Waves and Fields in Inhomogeneous Media*, Van Nostrand Reinhold, New York, 1990.
32. Yasumoto, K., H. Toyama, and T. Kushta, "Accurate analysis of two-dimensional electromagnetic scattering from multilayered periodic arrays of circular cylinders using lattice sums technique," *IEEE Transactions on Antennas and Propagation*, Vol. 52, No. 10, 2603–611, 2004, doi:10.1109/tap.2004.834440.
33. Toyama, H. and K. Yasumoto, "Electromagnetic scattering from periodic arrays of composite circular cylindrer with internal cylindrical scatterers," *Progress In Electromagnetics Research*,

Vol. 52, 321–333, 2005.

34. Toyama, H., K. Yasumoto, and T. Iwasaki, "Electromagnetic scattering from a dielectric cylinder with multiple eccentric cylindrical inclusions," *Progress In Electromagnetics Research*, Vol. 40, 113–129, 2003.
35. Kushta, T. and K. Yasumoto, "Electromagnetic scattering from periodic arrays of two circular cylinders per unit-cell," *Progress In Electromagnetics Research*, Vol. 29, 69–85, 2000.
36. Yasumoto, K., H. Jia, and H. Toyama, "Analysis of two-dimensional electromagnetic crystals consisting of multilayered periodic arrays of circular cylinders," *Electronics and Communications in Japan (Part II: Electronics)*, Vol. 88, No. 9, 19–28, 2005, doi:10.1002/ecjb.20182.
37. Yang, J., L.-W. Li, and C.-H. Liang, "Two-dimensional scattering by a periodic array of gyrotropic cylinders embedded in a dielectric slab," *IEEE Antennas and Wireless Propagation Letters*, Vol. 2, No. 1, 18-21, 2003, doi:10.1109/lawp.2003.810774.
38. Salary, M. M., M. Nazari, and H. Mosallaei, "Robust technique for computation of scattering and absorption of light by array of nanowires on layered substrate," *Journal of the Optical Society of America B*, Vol. 32, No. 12, 2448, 2015, doi:10.1364/josab.32.002448.
39. Yan, W.-Z., Y. Du, H. Wu, D. Liu, and B.-I. Wu, "EM scattering from a long dielectric circular cylinder," *Progress In Electromagnetics Research*, Vol. 85, 39–67, 2008.
40. Smith, G. H., L. C. Botten, R. C. Mcphedran, and N. A. Nicorovici, "Cylinder gratings in conical incidence with applications to woodpile structures," *Physical Review E*, Vol. 67, No. 5, 2003, doi:10.1103/physreve.67.056620.
41. Kan, D. J., A. A. Asatryan, C. G. Poulton, and L. C. Botten, "Multipole method for modeling linear defects in photonic woodpiles," *Journal of the Optical Society of America B*, Vol. 27, No. 2, 246, 2010, doi:10.1364/josab.27.000246.
42. Shanks, D., "Non-linear transformations of divergent and slowly convergent sequences," *Journal of Mathematics and Physics*, Vol. 34, No. 1–4, 1–42, 1955, doi:10.1002/sapm19553411.
43. Wynn, P., "On a device for computing the E M (S N) transformation," *Mathematical Tables and Other Aids to Computation*, Vol. 10, No. 54, 91, 1956, doi:10.2307/2002183.
44. Brezinski, C., Y. He, X.-B. Hu, M. Redivo-Zaglia, and J.-Q. Sun, "Multistep ε-algorithm, Shanks' Transformation, and the Lotka-Volterra system by Hirota's Method," *Mathematics of Computation*, Vol. 81, No. 279, 1527–549, 2012, doi:10.1090/s0025-5718-2011-02554-8.